Technical Article

Modelling of high temperature superconductors and their practical applications

***Abstract* — The paper deals with the modelling of high temperature superconductor (HTSC) bulks used in different levitation systems and electrical machines. The purpose of this paper is not the complete description of possible mathematical models of superconductors, but the presentation of chosen calculation algorithms used for development and optimization of field excitation systems and superconductors configurations in above applications only. The analysis presented in the paper is applied to several illustrative examples based on different practical configurations designed and built at the Institute for electrical Machines, TU Braunschweig, Germany (IMAB).**

I. INTRODUCTION

A new era in engineering materials opened when, 1986 Bednorz and Müller observed the superconductivity in lanthanum-barium-copper-oxide (LaBaCuO) at the critical temperature $T_c \approx 35$ K. The technological progress in the improvement of HTSC quality parameters (high critical current density J_c, high critical magnetic field H_c, domain size and homogeneity) has opened a wide range of possible applications of superconductor bulk material, such as magnetic bearings and electrical machines [8], [9], [17], [18], [21], [22], [29]. In this way "the HTSC products have moved from the laboratory curiosity to practical field-deployed systems" [11].
Fig. 1a shows exemplary 16 HTSC bulks manufactured within one batch-process, used in the levitation system of the flywheel in the Dynastore-Project [31]. The single typical HTSC bulk is illustrated in Fig. 1b.

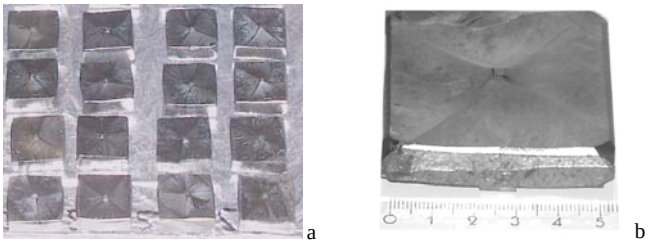

Fig. 1. High temperature superconductor bulks

The macroscopic mathematical modelling of above bulks and their application possibilities are the subject of this paper.

II. PRINCIPAL MACROSCOPIC MODELLS OF HTSC BULKS

The economical usage of any devices with HTSC bulks depends on the intensity of the external magnetic field and HTSC interaction. The wide range of possible field excitation configurations causes the necessity of different calculation methods/models formulation. These must be adequate enough to be applied while designing and optimizing HTSC systems. For the formulation of any model of superconductivity the classical vector potential definition has been used. In the 2D quasi-static case the magnetic vector potential **A** can be obtained from the Poisson equation (linear case)

$$\nabla^2 \mathbf{A} = -\mu_0 \mathbf{J} - \mathrm{rot}\mathbf{M}\,, \qquad (1)$$

where **J** denotes the current density vector and **M** the magnetization vector.

All calculation models of superconductivity use additionally different dependencies between the external magnetic field and current density distribution within the HTSC. These methods are based on the critical state model of Bean ([1], [2]): Elementary current densities within the HTSC are imposed to maintain the magnetic state unaltered inside the sample. The direction of the current densities depends on the local history of the applied magnetic field.
The main equations describing this state can be written in the form of the nonlinear dependencies:

$$\mathbf{J} = \frac{\mathbf{E}}{|\mathbf{E}|} J_c(\mathbf{B})\,, \text{ if } |\mathbf{E}| \neq 0 \qquad (2)$$

and

$$\frac{\partial \mathbf{J}}{\partial t} = \mathbf{0}\,, \text{ if } |\mathbf{E}| = 0\,. \qquad (3)$$

Depending on individual requirements, different possibilities to define advanced superconductivity models are available in order to determine the properties and characteristics of any practical configuration [32], [33], [34], [35]. The most important conditions which have to be defined are:

1. kind of transition to superconductivity: zero field cooling (ZFC) or field cooling (FC)
2. small or large displacements between HTSC and PM system
3. hysteretic behavior or not
4. static or dynamic interaction.

The proper description of the above conditions leads to one of the calculation models described below.
For solving of Eq. (1) the standard finite element method (FEM) has been applied (triangular elements, linear approximation). It leads to the fundamental system of algebraic equations of the form:

$$\mathbf{W}\mathbf{A} = \mathbf{U}\,, \qquad (4)$$

where **W** denotes the stiffness matrix and **U** the load vector.
Fig. 2 shows the typical iterative algorithm structure for the calculation of the HTSC-PM (permanent magnet) interaction.

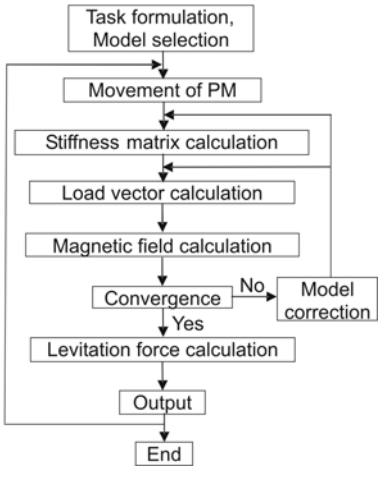

Fig. 2. Iterative algorithm for the calculation of the HTSC-PM interaction

The system (4) can be solved directly – typical number of unknowns by the fine discretization is of 100000.

A. Meissner model

The magnetic behaviour of type-I superconductors is characterised by the Meissner effect, where reversible surface currents are induced in the sample to perfectly screen the applied magnetic field. In HTSC such behaviour can be observed as long as the external field is lower than the first critical magnetic field H_{C1}. However, such perfect diamagnetic model may be used as a theoretical limit to design and optimise repulsive HTSC-PM configurations. Fig. 3 shows a superconductor in the magnetic field of a configuration used for superconducting magnetic bearings (flux concentrating arrangement). This calculation has been done introducing a very small value of the HTSC permeability $\mu_r \approx 0$ (Cartesian co-ordinates).

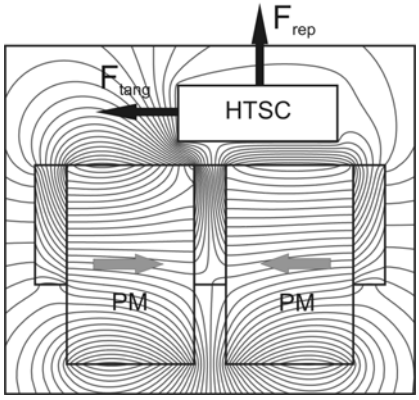

Fig. 3. High temperature superconductor bulk in the Meissner state

In the case of Fig. 3 both forces F_{rep} and F_{tang} are acting on the superconductor.

B. Trapped flux model

Type-II superconductors (known as the hard superconductors) allow some penetration by an external magnetic field into their region. This field can be trapped by a superconductor, when cooling below T_c. The trapped field distribution within the HTSC can be calculated by the numerical algorithm described in [19]. This algorithm requires that the field distribution in the initial position of HTSC and two field distributions of the Meissner state in the initial and final position of HTSC have to be determined. The final field distribution can be obtained as an appropriate combination of the vector potentials from these three initial calculation steps. Fig. 4 shows the superconductor in the initial (activation) position ($g=g_{act}$).

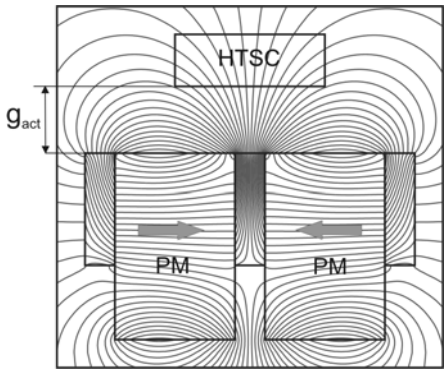

Fig. 4. HTSC bulk in the activation position $g=g_{act}$

The perfectly trapped magnetic field within the HTSC from the initial position (Fig. 4) in the final (displaced, operational) position has been depicted in Fig. 5.

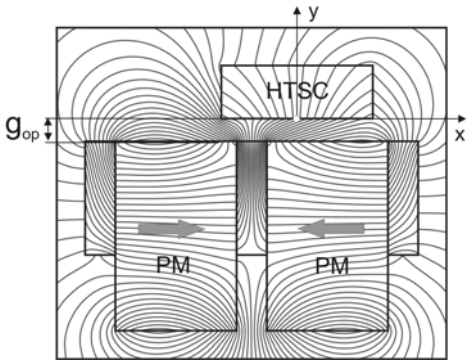

Fig. 5. High temperature superconductor bulk in the displaced (operation) position $g=g_{op}$

As can be seen from Fig. 5 the magnetic field within the HTSC remains unaltered and again, forces acting in both directions can be observed. Fig. 6 shows the current shell on the HTSC surface which screens the inner region of HTSC perfectly. The values of the surface current $\mathbf{J_s}$ can be determined from the field continuity condition at the interface between two media:

$$\mathbf{n} \times (\mathbf{H}_1 - \mathbf{H}_2) = \mathbf{J}_s , \qquad (5)$$

where $\mathbf{H_1}$ and $\mathbf{H_2}$ denote the magnetic field intensity vectors on the inner and outer side of the HTSC respectively.

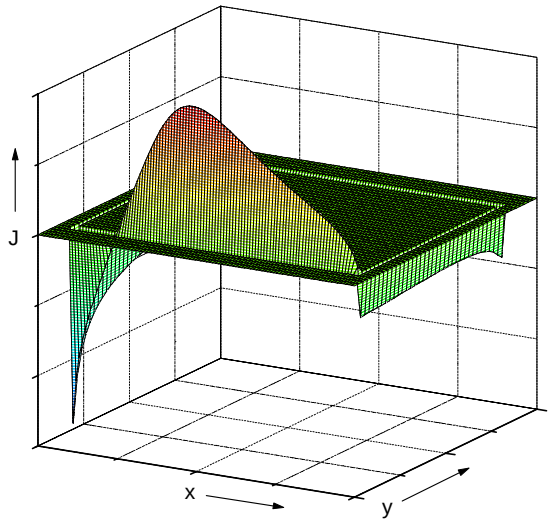

Fig. 6. Current shell in the HTSC from Fig. 5

Magnetization of YBCO superconductor bulk results in a strong superconducting permanent magnet (SPM).

Under assumption that the excitation system can be treated as perfect homogeneous in the direction of motion (z-, or φ-co-ordinate), all force calculations could be carried out in a two-dimensional plane orthogonal to the direction of movement. If however these simplified 2-D calculations have been compared with measurements, major differences could be observed. Even under the consideration of finite and even flux depending J_c-values, the discrepancies between measured and calculated force values are located in the 10% range. In reality neither the magnets of the excitation system nor the cluster of superconductor bulks are perfectly arranged as one uninterrupted unit. For further improvements of the force predictions the trapped flux calculation model has been extended for 3D-cases. Introducing the scalar potential V

$$\mathbf{H} = -\mathrm{grad} V , \qquad (6)$$

the following well known equation describing the 3D magnetic field is obtained:

$$\mathrm{div}(\mu \mathrm{grad} V) = \mathrm{div}(\mu \mathbf{H_J}) , \qquad (7)$$

where $\mathbf{H_J}$ denotes the source field strength.

Equation (7) can be used for the appropriate 3D-FEM formulation. The resulting system of algebraic equations has to be solved iteratively, because of its dimension (usually up to 600000-800000 unknowns for the required accuracy).

The extended 3D calculation model, developed at the IMAB, is able to consider imperfect excitation systems with not matching PMs and also interrupted iron structures. Furthermore, HTSC clusters composed of individual, electrically insulated HTSC bulks can be considered fore more sophisticated force determinations.

Fig. 7 shows the fundamental 3D field exciting configuration (flux concentrating arrangement), where the HTSC can be moved from one position to the other.

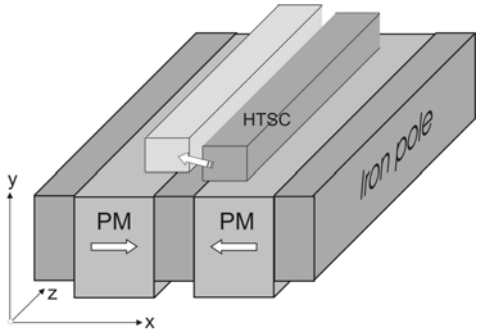

Fig. 7. HTSC and the field excitation system consisting of PMs and flux guiding iron parts

By means of this approach the 3-D field distribution (and all secondary quantities) in any HTSC-PM configuration by any possible movement of all parts of the system can be calculated.

The main drawback of the Meissner model or trapped flux model lies on their incapability to reproduce the hysteretic magnetic behaviour of type-II superconductors.

C. Vector Controlled Models

Fig. 8 shows the fundamental HTSC-PM configuration used for examination of different superconductivity calculation models. In the case of Fig. 8 the axis-symmetric FEM code has to be applied.

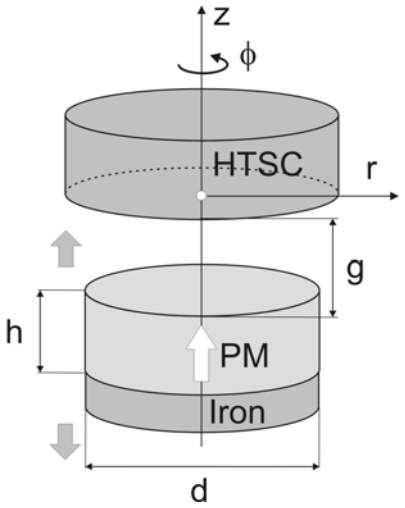

Fig. 8. Fundamental configuration for the examination of different calculation models (d_{HTSC}=30 mm, h_{HTSC}=15 mm, d_{PM}=d_{Fe}=25 mm, h_{PM}=20 mm, h_{IFe}=4 mm)

Measurements done for this configuration show hysteretic dependencies of the levitation force as a function of displacement for both: ZFC (trajectory: $g_{max}\rightarrow g_{min}\rightarrow g_{max}$) and FC (trajectory: $g_{min}\rightarrow g_{max}\rightarrow g_{min}$) activations (Fig. 9).

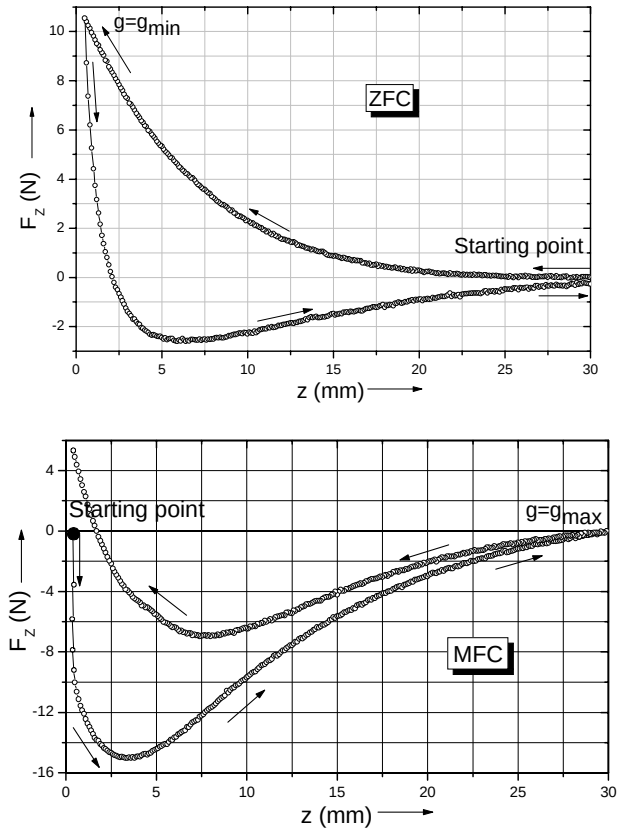

Fig. 9. a) Levitation force in ZFC process
b) Levitation force in FC process

To consider above hysteretic dependencies an additional iterative model of the superconductivity has been developed. This so called Vector Controlled J_c Model is based on the critical state model of the HTSC, where bulk currents in the sample are induced to avoid the variation of the magnetic flux within the material. In the superconducting region two degrees of freedom exist, namely the magnetic flux (both components) and the induced current density. An iterative process to obtain the final current density distribution which minimises the changes of the magnetic field within the HTSC by controlling the actual and previous magnetic field and current density distributions has been developed. By this method the current density distribution J_N in each calculation step is modified as:

$$J_N=J_c(B_N) \text{ if } |B_N-B_{N-1}| > \varepsilon \qquad (8)$$

and

$$J_N=J_{N-1} \text{ if } |B_N- B_{N-1}| < \varepsilon, \qquad (9)$$

where ε is an adaptive threshold correlated with the FEM-mesh size.

This method has been successfully applied to reproduce the hysteretic magnetic behaviour of HTSC. Modifications of this basic model lead to different similar algorithm which can be applied for different configuration, activation modes and required trajectories.

An interesting alternative to the above model is the “conductivity model” based on the analogy between the superconducting shielding currents and the eddy currents associated with conventional conductors. This approach allows iterative corrections of the artificial conductivities of the superconducting region:

$$\gamma_N=\gamma_{N-1}\, J_c/J_{N-1} \text{ and } \gamma_N=0 \text{ if } J_{N-1}<<J_c. \qquad (10)$$

Both models (and their different modifications) allow the determination of hysteretic levitation forces in the configuration from Fig. 8 for both ZFC and FC activation modes.

It has to be stated that the non-linear dependencies (2) and (3) can be used directly; resulting in the nonlinear equations set which can be solved by the Newton-Raphson method. Such approach has been successfully applied for the calculation of different HTSC-PM interactions [13].

The next figures show exemplary some calculation results obtained by different Vector Controlled Models.

Fig. 10 shows the magnetic field distribution within the HTSC at a small distance $g=g_{op}$ from the PM for the ZFC activation mode ($g_{act}\rightarrow\infty$), calculated by the VC Model under assumption that the superconductor reacts on the external magnetic field with the constant and known current density J_c.

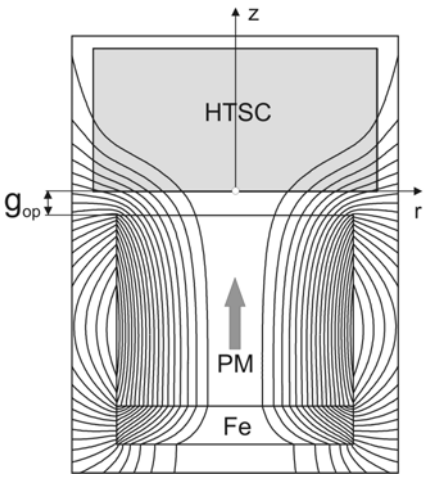

Fig. 10. Field distribution within the HTSC for the ZFC activation mode

The corresponding current density distribution within the HTSC is shown in Fig. 11.

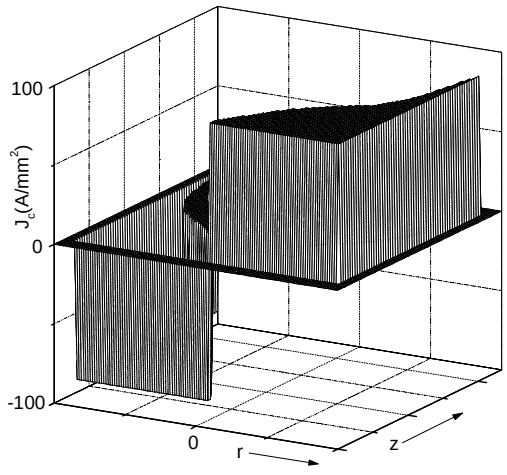

Fig. 11. Current density distribution within the HTSC from Fig. 10

In Fig. 11 the characteristic current density profile can be seen. In this position the superconductor remains non-saturated. It means that only a part of its region leads the critical current.

In the next step the HTSC is approaching to the activation system ($g=g_{min}$) and retreating again to $g=g_{op}$. The current density distribution within the HTSC for $g=g_{op}$ calculated by the conductivity model has been illustrated in Fig. 12.

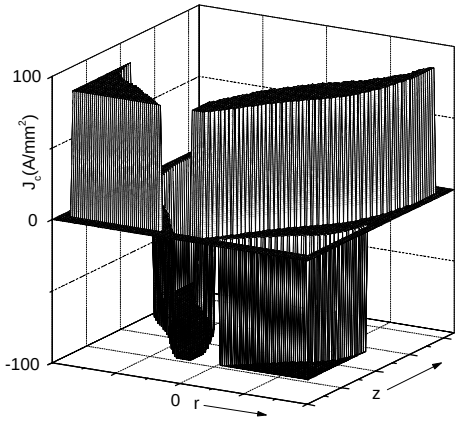

Fig. 12. Current density distribution within the HTSC $g=g_{op}$ calculated by the conductivity model (trajectory: $g_{act}\rightarrow g_{op}\rightarrow g_{min}\rightarrow g_{op}$)

As can be seen from Fig. 12 the current density changes its direction in some regions of HTSC – it results in smaller forces and finally leads to the hysteretic force dependency (Fig. 9a).

All above calculations have been performed under assumption that the critical current density is known. It means that this main quantity of each HTSC bulk has already been identified (s. chapter V). How important is the value of the J_c for each force calculation has been shown in Fig. 13 where the levitation force as the function of the critical current density has been presented (configuration from Fig. 8, FC activation).

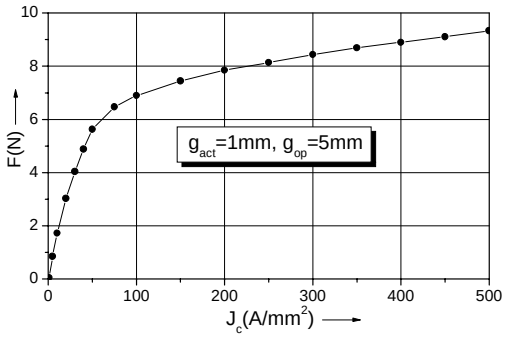

Fig. 13. Levitation force as the function of the critical current density for the configuration from Fig. 8 (FC activation)

The constant value of the critical current density does not guarantee the perfect agreement between measured and calculated force values. In order to obtain much better accuracy it was necessary to take into account different $J_c(B)$ dependencies for calculations. The best results have been obtained for function with the so-called fish tail effect (Fig. 14).

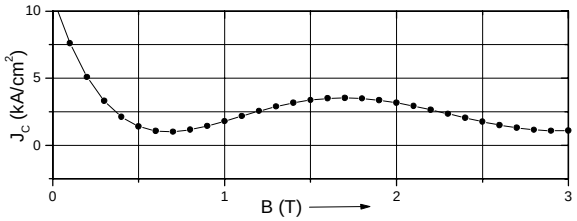

Fig. 14. $J_c(B)$ function with fish tail effect

The results of exemplary calculations using the $J_c(B)$-curve from Fig. 14 have been shown in the next figures. Fig. 15 illustrates the field plot in the multi-polar configuration for the ZFC activation mode ($g_{act}\rightarrow\infty$) at the position $g=g_{min}$.

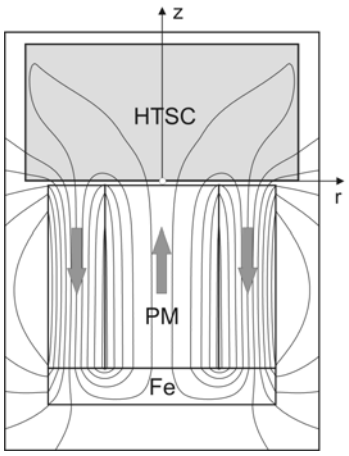

Fig. 15. Field distribution within the HTSC for ZFC activation mode ($g_{act}\rightarrow\infty$)

The resulting current density distribution within the HTSC is shown in Fig. 16.

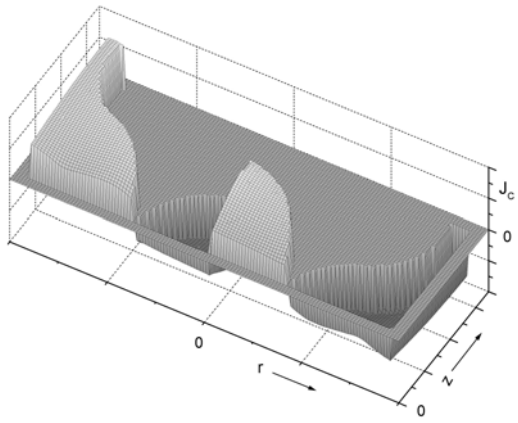

Fig. 16. Current density distribution within the HTSC from Fig. 15

After testing of all possible calculation algorithms for the fundamental configuration from Fig. 8, they can be applied for calculations of any practical configuration used. The next picture shows exemplary the field distribution calculated by the VC Model for the configuration from Fig. 4 used for superconducting bearings.

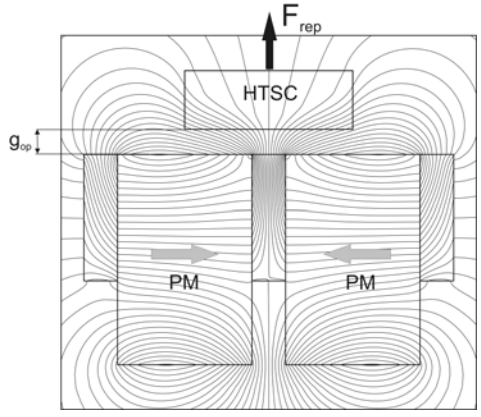

Fig. 17. Field distribution in the flux concentrating arrangement from Fig. 4 calculated by the VC Model

For practical calculation (especially for superconducting bearings) a hybrid method, which combines both the VC Model and the trapped flux model can be applied. The first one is used to compute the current density distribution within the HTSC as the activation process takes place. The trapped flux model can be applied for the force and stiffness calculation for small displacements in the neighbourhood of the operating position.

D. Flux creep and flux flow

The Vector Controlled Model can be modified in order to include the effect of the flux flow and flux creep phenomena. In this way some dynamical effects of HTSC-PM interaction can be evaluated, such as the force decay and frequency dependence of the stiffness and damping constants ([27], [29], [28]).

III. Superconducting magnetic bearings

According to the classical theorem of Earnshaw, it is impossible to attain stable equilibrium in a system in which only inverse-square-law forces are acting [12]. This theorem has been extended by Braunbeck [4] for systems containing a diamagnetic material ($\mu_r<<1$) and by Bevir [3] who proposed a superconducting magnetic bearing with a ferromagnetic reaction part. The inherently stable levitation has been also observed for HTSC bulks in magnetic field.

Superconducting magnetic bearings (SMBs) are one of the most promising applications of bulk high-T_c superconductors. They are based on inherently stable force interaction between a field excitation system and HTSC bulks. The special merits of these bearings are: Contact free and inherently stable operation from stand still up to highest speeds, no wear out, no need for control- and sensor-units, high reliability and no EMC-problems. Of outstanding interest is their use for high speed machines e.g. turbo machinery, or rotating energy storage systems and for linear and two dimensional planar transport systems ([5], [6], [8], [9], [17], [18], [21], [22], [27], [28], [29], [30], [31]). SMBs are very convenient for applications with extreme requirements operating under clean room or vacuum environment.

For the design of a SMB there are two different basic topologies for the arrangement of the HTSC and the PM-excitation system available (Fig. 18). Depending on its characteristics each of them is predestined for a particular kind of application.

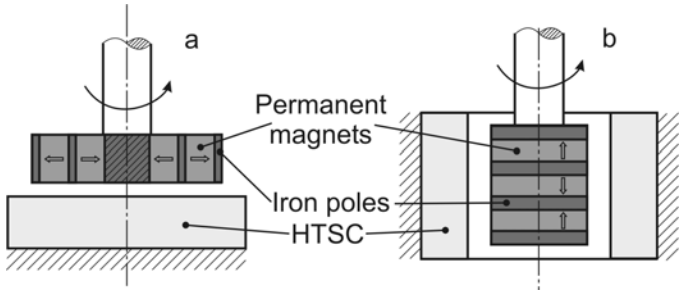

Fig. 18. Fundamental HTSC-bearing topologies
a) Planar bearing b) Cylindrical bearing

The axial or thrust bearing (Fig. 18a), specially in a linear version, is suited for levitation and guiding tasks as they appear in transportation systems or, in a circular arrangement, for flywheel energy storage systems [28]. The cylindrical (Fig. 18b) bearing can be used for rotating machine parts like shafts and high speed rotors. In both configurations, the fundamental flux concentrating structure from Fig. 5 can be seen. Basing on these principal topologies, within several research projects (founded by the German federal government) SMBS for contact-less transport system and turbo machines have been designed and tested.

For each HTSC-PM structure there are different activation modes possible:

1. ZFC (zero field cooling): $g_{act} >> g_{op}$,
2. OFC (operational field cooling): $g_{act} = g_{op}$,
3. OFCo (operational field cooling with offset): $g_{act} \approx g_{op}$,

4. MFC (maximum field cooling): $g_{act} \approx 0$ mm.

For the OFC activation the SMB operates in the same position in which it is cooled. This occurs under zero gravity conditions in the free space, or if the weight is compensated by other device. The typical activation mode for SMB is OFCo, where the operational position of HTSC differs minimally from the activation position. For MFC and ZFC activation there is mostly not enough space in the bearings air gap.

For the dimensioning of a SMB the following parameters have to be known:

1. Static forces – radial and axial
2. Stiffness matrix
3. Damping matrix
4. Frequency dependence of stiffness and damping.

All these quantities of the SMB can be numerically calculated and optimized by using of the appropriate algorithm described above.

Fig. 19shows the test bench for the superconducting bearings (built at the IMAB), consisting of the high speed motor, radial and axial actuators and the cryocooler.

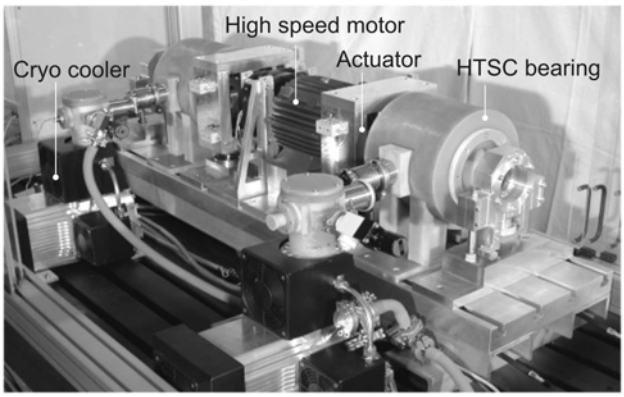

Fig. 19. Photo of the test bench for the SMB

The structure of the SMB used for in the above test set-up has been shown in Fig. 20.

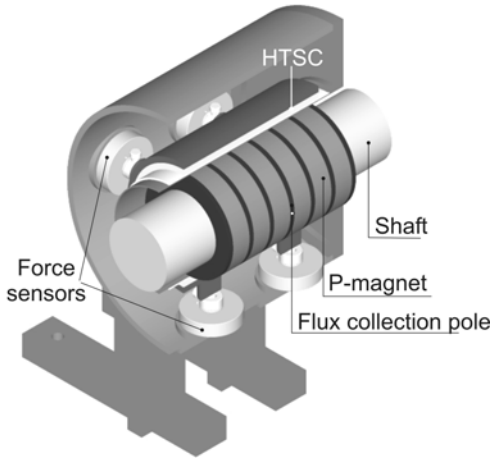

Fig. 20. Design of the SMB consisting of a cylindrical copper cold head with HTSC bulks in a Dewar and an excitation system in the warm bore

The field excitation system is a cylindrical multi-polar arrangement with six axial magnetized ring shaped PMs and seven iron poles as flux concentrators (Fig. 21b). It is mounted on the shaft and operated under ambient conditions in a warm bore of the Dewar for the HTSC.

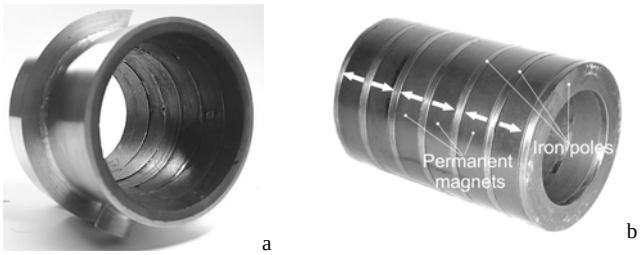

Fig. 21. a) Cooper cold head with HTSC bulks
b) Cylindrically shaped excitation system for radially acting SMB composed of alternating axially magnetized PMs located between cylindrical iron poles (Fig. 18b)

The mechanical air gap width is reduced by a super-insulation consisting of the housing and a multi-layer foil insulation. Surrounding the thermal insulation the HTSC is fitted into a copper tube that insures a constant temperature distribution and also stabilizes the HTSC tube mechanically. Directly attached to the copper tube are four force sensors – two horizontal and two vertical. The cooling of the HTSC is provided by a one step Stirling-type refrigerator which is connected to the copper tube via a flexible copper wire. A cryo-vacuum pump is attached to the cold head of the machine and provides the insulating vacuum during operation.

The activation of the bearing is done by using two lifting devices that also contain the auxiliary bearings. Before cooling down the HTSC, the rotor is lifted to an empirically determined offset relative to the operating position. The rotor is released when the operating temperature below T_c is reached. Due to its mass the rotor sinks down to operating position (Fig. 22).

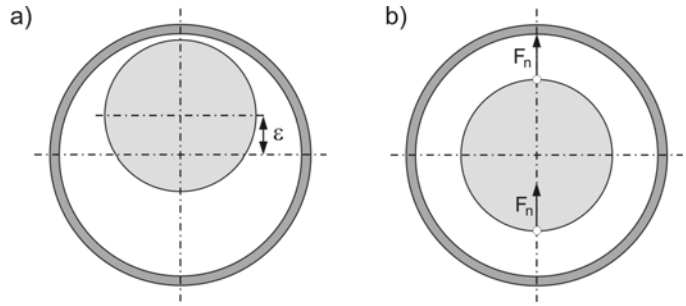

Fig. 22. Activation of a cylindrical bearing:
a) Cooling position, b) Operating position

The bearing geometry depicted in Fig. 20 ($d_{i,HTSC} = 90$mm, $\delta = 4$mm, $l = 124$mm) provides the static levitation force of $F_y = 483$N and a stiffness of $k_y = 309$N/mm at the operation position.

The obtainable preloading of the bearing is limited by the width of the air gap and the rotor mass. If higher values of levitation force and stiffness are required, another activation set-up for activating of the bearing has to be applied. At the IMAB a method of activation is developed allowing the adjustment of the air gap without changing the rotor position (Fig. 23). The activation can be done by spreading the HTSC shells, cooling down below T_c and then adjusting the air gap to the operational value. This gives the opportunity to adjust different air gaps for the upper and the lower shell. Such design enables applications that do not allow a displacement of the rotor position, i.e. turbo machinery, because of very small runner clearance

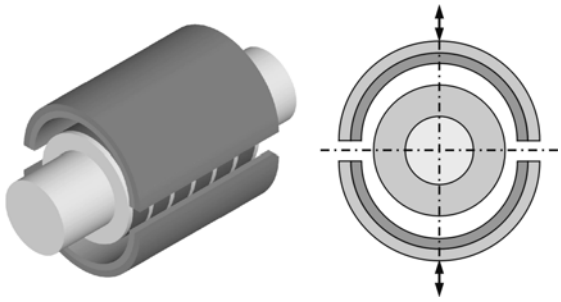

Fig. 23. Activation by the displacement of splitted HTSC shells

Configuration from Fig. 3 can be used for contact-less linear transport. A similar arrangement can be applied for the suspension of the flywheel Fig. 24.

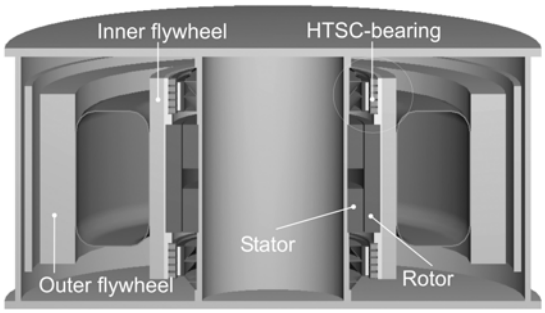

Fig. 24. Flywheel as an energy storage with radial SMBs (Dynastore-Project [30], [31])

The details of the superconducting bearing have been shown in Fig. 25.

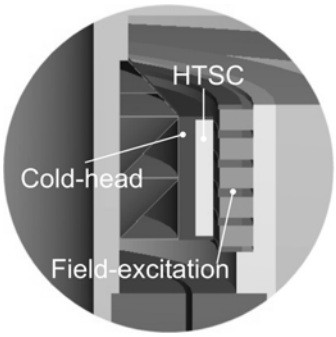

Fig. 25. Radial superconducting bearing for the flywheels from Fig. 24

The flywheel from Fig. 24 can also be supported by the axial bearing illustrated in Fig. 26.

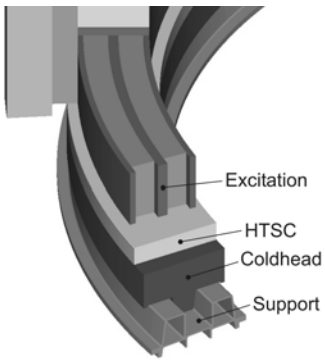

Fig. 26. Axial superconducting bearing for flywheels

Another planar superconducting magnetic bearing without degrees of freedom has been developed for the contact-free support of double walled container for the liquid H_2 transport Fig. 27.

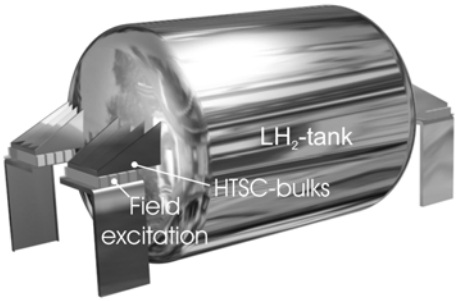

Fig. 27. Inner part of the double walled LH_2 cryocontainer for automotive applications

The excitation system for the above SMB has been shown in Fig. 28a. The magnetic field distribution of the excitation system (Fig. 28b) and the forces acting on the HTSC have been determined by the 3D approach (7).

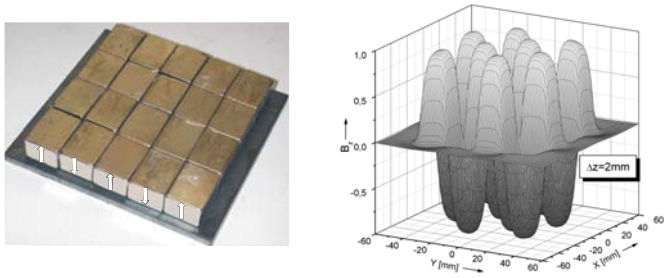

a b

Fig. 28. a) Chess board formed planar excitation system
b) 3D field distribution with an utmost increased field gradient to achieve enhanced force densities

IV. USE OF HTSCS IN ELECTRICAL MACHINES

By far the greatest portion of primary energy is directly or indirectly converted into mechanical energy by machines or actuators for automobiles, planes or machine tool drives. Thus the enhancement of effectiveness of the energy conversion is of great importance for economical and environmental reasons. Newest improvements of HTSCs regarding the increase of the critical current density J_c and the field trapping capability encourage the application of this material in electrical machines with highly improved performance data.
The use of the HTSC material in electromechanic energy converters has been described in many papers ([7], [15], [20], [24]). HTSC bulk material can be applied in electrical machines as field screens and as superconducting magnets (SPM).
Superconducting magnetic screens are used for reduction of the parasitic stray field and for the focusing of the main magnetic field. It has been demonstrated in Fig. 29, where the HTSC-screens have been used for both: Intensifying of the armature field and for the suppression of the armature.

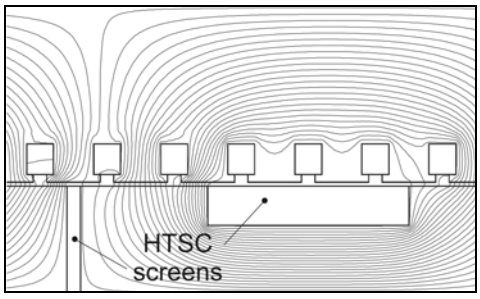

Fig. 29. 1. Field distribution of a poly-phase reluctance machine with individual HTSC-screens in the inert-pole region and pole slot

The rotor of the machine depicted in Fig. 30 consists of alternate iron and superconducting plates. The use of HTSC screens increases the torque of 50-100% [24].

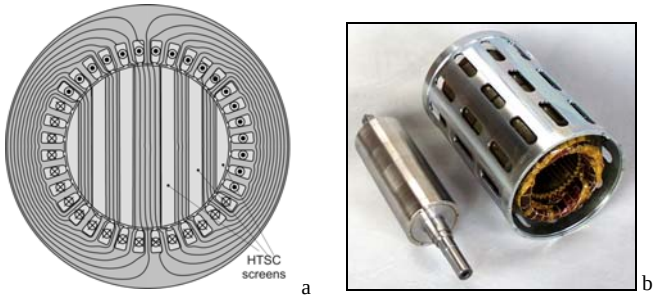

Fig. 30. "Zebra" construction of a poly-phase reluctance machine
a) Field plot
b) Disassembled 200kW machine with reinforced rotor structure. (OSWALD Elektromotoren GmbH)

Trapped field machines can benefit fully from the advantages of superconductivity if they can magnetized to significantly higher air gap inductions than possible with conventional permanent magnets e.g. up to 2 T. In general two main modes of magnetizing of HTSC in electrical machines can be defined:

1. Magnetization of the cooled HTSC bulks by operational armature currents,
2. Magnetization of the cooled HTSC bulks by impulse discharge of a capacitor.

Assuming the magnetization of HTSC can be achieved with acceptable technical effort, the very high air gap inductions enable the increasing of the air gap. This zone can completely be used for the armature windings. This leads to the slot-less synchronous machines designs with reduced winding resistances (comparable with machines with superconducting windings). Because of the reduction of the armature reaction these machines exhibit extremely high short overload capability.

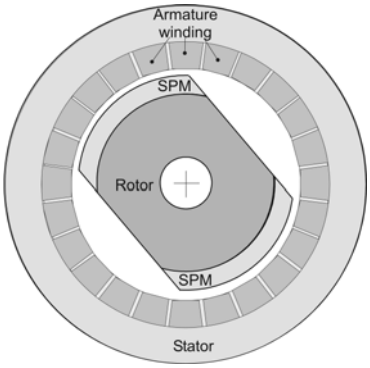

Fig. 31. Slot-less synchronous machine with the air gap oriented SPM excitation

The principal 3D structure of the gap oriented arrangement with SPM has been shown in Fig. 32.

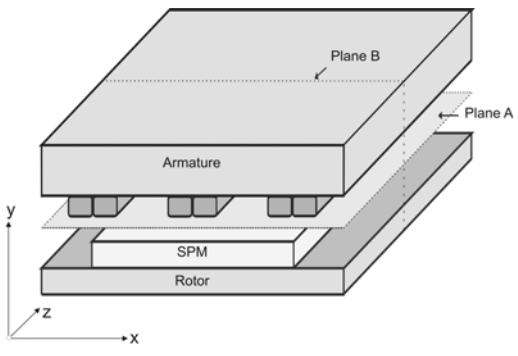

Fig. 32. 3D-structure for a HTSC-excited synchronous machine

For the optimization of machines depicted in Fig. 32 the 3D-approch (7) can be used.

V. QUALITY ESITMATION OF HTSC-BULKS

The manufacturers of HTSC-bulk material are faced with two major demands. At first for applications of superconducting permanent magnets composed of many bulks in form of a cluster, the critical current density J_c has to be increased as high as possible, so that surfaces of adjacent HTSC-bulks with currents in an opposite direction compensate each other with the effect of the homogenous excitation field distribution. A second demand on the HTSC-quality is related to the producible block-size without internal sub-domains. With respect to the total flux, an increased block size with reduced J_c may be replaced by a cluster of several high quality SPM-blocks of minor size. The knowledge of the material parameters e.g. domain sizes, positions and orientations together with the values of their internal J_c are of a great importance for the design of above mentioned machines.

The internal structure of commercially available superconducting bulks is strongly related with the manufacturing process (top-seeded melting), implicating that the orientation of the crystallographic a-b planes can not be ensured for arbitrarily large pellets. At a certain distance from the seed, the planes may loose their orientations and the material solidifies in disoriented directions of the a-b-planes. It means that HTSC-bulks exhibit usually a non-homogeneous internal structure with unknown positions and orientations of superconducting sub-domains. For each industrial application it is of great importance that all used HTSC-bulks in a cluster are of the same quality.

To control the quality after the fabrication the HTSC will be inserted into the bore of a high field magnet of several Tesla and then cooled below the critical temperature T_c. Thus magnetically saturated the magnetic flux will be trapped within the HTSC by internal currents after the switch-off of the external field. Fig. 33 shows the magnetic field distribution measured at the distance of 2 mm above the HTSC surface for two superconductors of different quality.

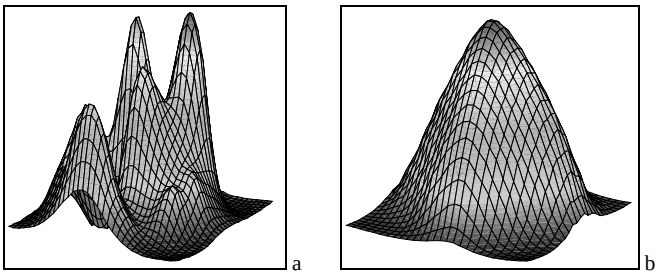

Fig. 33. Distribution of the magnetic field (normal component) trapped by HTSC-bulks of different quality in the saturated Shubnikov state (measured at 2 mm above the surface)
a) HTSC-bulk composed of several sub-domains
b) Single grain HTSC-bulk

The field distributions shown in Fig. 33a and b differ markedly as the left HTSC-bulk consists of several small sub-domains whereas the right one exhibits the field of a perfect single domain HTSC which is significant for high quality bulk material. The values of the flux density components can be applied for the determination of the J_c distribution within the HTSC and thus for their quality control.

Fig. 34 shows the SPM from Fig. 4 after removing of the excitation system. By the use of all components of the external field in the close neighborhood of the HTSC known from measurements (region G_0), the current distribution within the sample can be identified.

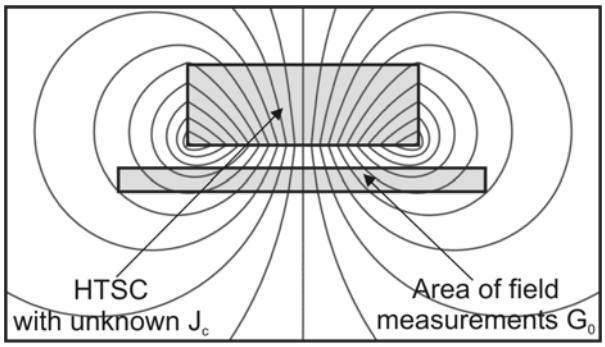

Fig. 34. SPM from Fig. 4 in the absence of the activation system

Identification of the current distribution within the sample by the use of the external field values constitutes a typical inverse field problem and belongs to the class of the improperly posed problems. That is, its solution may not be unique, nor continuous to the input data, thus the standard numerical field calculation method can not be applied directly to the identification of the current density distribution within HTSC [10], [25], [26].

To solve this problem the fundamental finite element equation set (4) has been extended by equations describing the magnetic field in regions of field measurements G_0:

$$\mathbf{B(x,y) = B_0} \text{ w } G_0. \tag{11}$$

This leads to a modified, linear, over-determined and ill-conditioned set of equations with two unknowns: vector potential values in the whole region and current density values within the superconductor

$$\mathbf{W_M A_M = U_M}\,. \tag{12}$$

Since the coefficient matrix $\mathbf{W_M}$ is of the size $m \times n$ ($m>n$), the solution of the equation set exists in the sense of the least squares:

$$A_0 = \min \left\| \mathbf{U_M} - \mathbf{W_M A_M} \right\| \tag{13}$$

This solution can be written as

$$\mathbf{A_0 = R U_M}\,, \tag{14}$$

where **R** denotes the Moore-Penrose pseudo-inverse [16].

The minimal least squares solution, i.e. the vector of minimum Euclidean length which minimises (13) can be computed by the singular values decomposition of $\mathbf{W_M}$ that enables the calculation of the appropriate Moore-Penrose pseudo-inverse **R** and the minimal least squares solution $\mathbf{A_0}$ of the problem. It should be noted here that the numerical implementation of the above algorithm is very difficult because of the possible numerical instabilities. Therefore it is necessary do define several accuracy criterion to prevent convergence to solutions with unacceptable values.

The real superconductor is usually composed by some sub-domains which can carry the current of high magnitude and others with decayed properties with respect to their internal J_c (drastically shown in Fig. 33a). As the knowledge of the continuous J_c distribution is not so essential for the force determination, thus from the practical point of view it is necessary to define the average current density values for some bigger sub-regions of the HTSC only. This simplifies the calculation process and gives the required information about the distribution of superconducting domains within the HTSC. The mean value of the determined current density in each sub-region can be called the "engineering current density", as only this value is responsible for the force interaction between the HTSC and any external magnetic field. Thus, according to the required accuracy, the superconducting region has been artificially divided into some separated parts (rings for the axis-symmetric case) with identical cross-sections and the individual mean J_c value for each individual part has been determined. By this approach the number of unknown J_c density values has been advantageously reduced. This reduces at the same time the extension of the measurement area, leading finally to much smaller equation sets and stabilising the calculation process.

This method can be extended for the 3D case. Because of the size of the over-determined equation set it is possible to apply the above algorithm for very simple structures only (single superconductors without iron parts). To define the mathematical model for the 3D quality testing the superconducting bulk has been artificially divided into N identical shaped sub-cubes with three individual current sheet values and directions J_c surrounding each cube. This is based on the critical state model (Meissner-state) of HTSC, which is applied to these small sub-elements. The magnetic field distribution of such cubes can be calculated by the Biot-Savart law. Using the Biot-Savart formulas the components of the magnetic field in each point of the outer area can be determined. The mapping: Current density distribution within the HTSC $\rightarrow$ magnetic field distribution in any region leads to a linear, over-determined and ill-conditioned set of P equations (P - number of evaluation points) with 3N unknown surface current densities (P>>N). This equation set can also be solved by the least squares method [26].

The proposed identification codes have been validated by many experiences and thus may serve as a non-destructive quality evaluation algorithm for single HTSC bulk pieces or even clusters consisting of many bulks as used for magnetic bearings and the excitation of electrical machines. The above algorithms have been used for the quality testing of HTSC-bulks used at the Dynastore-Project (Fig. 1b).

VI. References

[1] Bean C. P., "Magnetisation of hard superconductors", *Physical Review Letters* 8, (1962), p. 250

[2] Bean C. P. "Magnetitisation of high-field super conductors", *Review Modern Physics* 36 (1964), pp. 31-39

[3] Homer G.J., Randle T.C., Walters C.R., Wilson M.N. and Bevir M.K., "A new method for stable levitation of an iron body using superconductors", *J. Phys. D: Appl. Phys*., Vol. 10, 1977, p. 879-886

[4] Braunbeck W., "Freely Suspended Bodies in Electric and Magnetic Fields", *Z. Phys*., 1938, Vol. 112, p.753-763

[5] Canders W.-R., May H., „Magnetische Lagerung eines Rotors in einem Stator", Deutsches Patent DE 197 27 550 C2

[6] Canders W.-R., May H., „Magnetische Lagerung", Deutsches Patent DE 100 34 922 C2

[7] Canders W.-R., May H., Palka R., Portabella E., "Machines with high temperature superconducting bulk material in comparison with permanent magnet excited synchronous machines", ICEM'2000, Helsinki

[8] Canders W.-R., May H., Palka R., "Topology and performance of superconducting magnetic bearings", *COMPEL* 17, 5/6, 1998, pp. 628-634

[9] Canders W.-R., Hoffmann J., May H., Palka R., "SMB design based on advanced calculation methods validated by practical experience", ISMB9'2004, Lexington KY, pp. 7-12

[10] Canders W.-R., May H., Palka R., "Identification of the current density distribution of monolithic superconductors", ISTET'97, Palermo
[11] Chase D. R., "High-temperature superconductors: online and operational", *RF DESIGN BULLETIN*, June 2002
[12] Earnshaw S., "On the Nature of the Molecular Forces which regulate the Constitution of the Luminiferous Ether", *Trans. Cambridge Phil. Soc.* Vol. 7 (1842), pp. 97-112
[13] Hofmann C., Ries G., "Modelling the interactions between magnets and granular high-Tc superconductor material with a finite-element method", *Supercond Sci. Technol.* 14 (2001) 34-40
[14] Kordyuk A. A., "Magnetic levitation for hard Superconductors", *J. Appl. Phys.* 83 (1), January 1998
[15] Krabbes G., Fuchs G., Canders W.-R., May H., Palka R., *High Temperature Superconductor Bulk Materials*, WILEY-VCH (to be printed)
[16] Lawson C.L. and Hanson R.J., *Solving least squares problems*, Prentice-Hall 1974
[17] Lee P. J., *Engineering superconductivity*, Wiley&Sons, 2001
[18] Ma K.B., Postrekhin Y.V., Chu W.K., "Superconductor and magnet levitation devices", *Rev. Sci. Instrum.*, Vol. 74, No. 12, 2003
[19] May H., Palka R., Portabella E., Canders W.-R., "Evaluation of the magnetic field–high temperature superconductor interactions", *COMPEL* 2004, Vol. 23, No. 1, pp. 286-304
[20] May H., Palka R., Portabella E., Canders W.-R., "Calculation of the properties of electrical machines with high temperature superconducting bulk material", ECCOMAS'2000, Barcelona
[21] Moon F.C., *Superconducting Levitation*, Wiley&Sons, 1994
[22] Murakami M., *Melt processed high-temperature superconductors.* Word Scientific 1992
[23] Neittaanmäki P., Rudnicki M. And Savini A., *Inverse problems and Optimal Design in Electricity and Magnetism*, Clarendon Press, Oxford 1966
[24] Oswald B., Strasser T., Krone M., Soell M., Oswald J. and Best K.J., "Superconducting motors with HTS bulk material for medium power range", EUCAS'1999, Sitges
[25] Palka R., "Synthesis of magnetic fields by optimization of the shape areas and source distributions", *Archiv für Elektrotechnik* 75 (1991) 1-7
[26] Palka R., May H., Canders W.-R., "Nondestructive quality testing of high temperature superconducting bulk material used in electrical machines and magnetic bearings", *Optimization and Inverse Problems in Electromagnetism*, Kluver Academic Publishers 2003, pp. 303-312
[27] Portabella E., Palka R., May H.,. Canders W.-R., "Influence of vibrations in HTSC-PM bearings. Computations and experiments" *COMPEL* 2000, Vol. 19, No. 2, pp. 724-729
[28] Portabella E., Palka R., May H.,. Canders W.-R., "Static and dynamic model of a HTSC axial bearing", ISMB 2000, Zurich
[29] Portabella E., *Static and Dynamic Properties of High Temperature Superconducting Bearings*, PhD-Thesis, Braunschweig 2000
[30] Siems S.O., *Konstruktion von Magnetlagern mit Hochtemperatursupraleitern*, PhD-Thesis, Braunschweig 2003
[31] Siems S.O., May H. and Canders W.-R., "Levitation forces and stiffness of model arrangements of magnetic HTSC bearings", ISMB 2002, Mito
[32] Tsuchimoto M., Kojima T., Takeuchi H. and Honma T., "Numerical analysis of levitation force and flux creep on high T_c superconductor", IEEE *Transactions on Magnetics* 29, 1993, pp. 3577-3579
[33] Tsuchimoto M., Takeuchi H. and Honma T., "Numerical analysis of levitation force on a high T_c superconductor for magnetic field configuration", *Transactions of the IEE of Japan*, 114-D, 1994, pp. 741-745
[34] Tsuchimoto M., Kojima T. and Honma T., "Numerical analysis of frozen field model for levitation force of HTSC", Cryogenics 34, 1994, pp. 821-824
[35] Yoshida Y., Uesaka M. and Miya K., "Magnetic field and force analysis of high T_c superconductor with flux flow and creep", *IEEE Transactions on Magnetics* 30, (1994), pp. 3503-3506

ACKNOWLEDGMENT

The author wishes to express his indebtedness to the work of his colleagues at the Institute of electrical Machines, TU Braunschweig, Germany, in particular Mr. Hardo May for the cooperation and his excellent ideas.

AUTHORS NAME AND AFFILATION

Ryszard Palka
Chair of Theoretical Electrotechnics and Computer Science
Technical University of Szczecin
Ul. Sikorskiego 37
70-310 Szczecin, Poland
e-mail: r.palka@web.de